https://doi.org/10.5194/egusphere-2025-6315
Preprint. Discussion started: 28 December 2025
© Author(s) 2025. CC BY 4.0 License.

Extreme Mediterranean cyclones under future climate change

Onno Doensen[1,2], Martina Messmer[3], Edgar Dolores-Tesillos[4], and Christoph C. Raible[1,2]

[1]Climate and Environmental Physics, University of Bern, Bern, Switzerland
[2]Oeschger Centre for Climate Change Research, University of Bern, Bern, Switzerland
[3]Geoscience and Remote Sensing, Faculty of Civil Engineering and Geosciences, Delft University of Technology, Delft, The Netherlands
[4]Faculty of Geosciences and Environment, University of Lausanne, Lausanne, Switzerland

Correspondence: Onno Doensen (onno.doensen@unibe.ch)

Abstract. The Mediterranean storm track is characterized by small but intense cyclones that can cause extreme weather events across the region. Thus the aim of this study is to investigate the impact of future climate change on extreme wind, precipitation and compounding cyclones. Using a regional climate model simulation, we show that the mean cyclone frequency is reduced by roughly a third in the Mediterranean by the end of the 21st century under the representative concentration pathway RCP8.5. For precipitation-type extreme cyclones (EXCs), future projections show increased precipitation during their most intense phase in the western Mediterranean (WMED), whereas precipitation from these cyclones remains similar in the eastern Mediterranean (EMED). Moreover, precipitation EXCs in the EMED are shifted southward, whereas the latitude of precipitation EXCs in the WMED remain unchanged in the future. The intensification of WMED precipitation EXCs in the future is partly explained by a significant increase in diabatically produced PV during their mature phase. Wind speed EXCs become more intense in both the WMED and EMED in the future under RCP8.5. The reason for this intensification is that wind speed EXCs in the future are located on the left exit of the jet streak, the latter also being intensified in the future. The future change of compounding precipitation and wind speed cyclones is similar to the individual precipitation and wind speed EXCs, with the exception that wind speed of compounding EXCs is reduced in the EMED. Thus, we find that despite a general reduction of cyclones in the Mediterranean, precipitation and wind speed EXCs intensify in the future in some areas, which implies strong socio-economic consequences for the Mediterranean.

1 Introduction

The Mediterranean has long been recognized as one of the most active cyclogenesis regions in the world (Pettersen, 1956). Due to the unique location and topography of the Mediterranean Basin, cyclones in the Mediterranean tend to be of smaller scale, shorter lifetime, and lower intensity compared to cyclones in the main storm track regions of the Atlantic and Pacific (Trigo, 2006; Campa and Wernli, 2012; Flaounas et al., 2014). Yet, these cyclones can heavily impact the Mediterranean region as a result of heavy precipitation events (Pfahl and Wernli, 2012; Flaounas et al., 2015a; Raveh-Rubin and Wernli, 2015), heavy windstorms (Nissen et al., 2010; Raveh-Rubin and Wernli, 2015), and coastal floods (Lionello et al., 2019; Ferrarin et al., 2021). When these hazards co-occur as compound extremes, they can have a larger impact than the individual events combined

https://doi.org/10.5194/egusphere-2025-6315
Preprint. Discussion started: 28 December 2025
© Author(s) 2025. CC BY 4.0 License.

(Martius et al., 2016; Zscheischler et al., 2018; Messmer and Simmonds, 2021; Vakrat and Hochman, 2023; Givon et al., 2024; Portal et al., 2024). Moreover, the Mediterranean is projected to be heavily influenced by future climate change and is defined as a "climate change hotspot" (IPCC, 2021).

The impact of climate change on Mediterranean cyclones has been extensively studied in global circulation models (GCM) (e.g. Lionello et al., 2002; Raible et al., 2007; Nissen et al., 2014; Hochman et al., 2020; Doensen et al., 2025). For example, Zappa et al. (2014) showed that CMIP5 models can realistically resolve the cyclone tracks and cyclone-related precipitation within the Mediterranean. GCMs also project a robust reduction in future cyclone frequency in the Mediterranean (e.g. Raible et al., 2010; Ulbrich et al., 2013; Nissen et al., 2014). Raible et al. (2010) showed evidence that this reduction is due to a decrease in baroclinicity and an increase in static stability. Nissen et al. (2014) showed that the decrease can also be related to a positive shift in the North Atlantic Oscillation (NAO).

In the Mediterranean, a decrease in winter precipitation has already been observed in the 20th century (Trigo et al., 2000) and the region is projected to become even drier in winter in the future (Zappa et al., 2015). Most of the precipitation in the Mediterranean occurs in the vicinity of a cyclone (Pfahl and Wernli, 2012), and hence this future reduction in precipitation is most likely caused by a reduction in cyclones. Precipitation extremes occur mostly in the autumn in the western Mediterranean and in winter in the eastern Mediterranean (Raveh-Rubin and Wernli, 2015). Reale et al. (2021) showed that cyclone-related precipitation may increase in the western Mediterranean and decrease in the eastern Mediterranean in the future, indicating a discrepancy within the Mediterranean itself. However, Chericoni et al. (2025) showed that future extreme cyclone-related precipitation may increase in intensity despite a reduction in average cyclone-related precipitation and the number of extreme cyclones. Wind extremes occur mostly in winter for both the western and eastern Mediterranean (Raveh-Rubin and Wernli, 2015). Most climate models show a decrease in cyclone-related wind speed for the Mediterranean in the future (Zappa et al., 2013; Reale et al., 2021; Dolores-Tesillos et al., 2022), however the confidence of the projections on the impact of climate change on extratropical cyclone wind speeds is low (Catto et al., 2019).

To interpret these projected shifts in Mediterranean cyclone behaviour, it is essential to analyse the underlying processes. For example, diabatic processes can substantially enhance the cyclonic circulation in an extratropical cyclone by low-level potential vorticity (PV) production (Davis and Emanuel, 1991). Additionally, intrusion of stratospheric high PV air plays an important role in the formation and dynamics of Mediterranean cyclones (Raveh-Rubin and Flaounas, 2017; Scherrmann et al., 2024). As a result, Mediterranean cyclones are often the result of an interplay between baroclinicity and diabatically produced PV (Homar et al., 2002; Fita et al., 2006). Nevertheless, Mediterranean cyclones are less deep than extratropical cyclones in the main storm track regions and only develop PV anomalies of moderate intensity (Campa and Wernli, 2012). Low-level diabatically produced PV is often the dominant source of PV in Mediterranean cyclones (Scherrmann et al., 2023), hence increased latent heating in a warmer climate may lead to cyclone intensification due to increased low-level diabatic PV production (Büeler and Pfahl, 2019), especially impacting wind speeds in the warm sector (Priestley and Catto, 2022). Moreover, Zhang and Colle (2018) suggested that future extratropical cyclones may be less intense in their initial phase due to lower baroclinicity in the atmosphere, but more intense in their mature phase due to increased diabatically produced PV.

https://doi.org/10.5194/egusphere-2025-6315
Preprint. Discussion started: 28 December 2025
© Author(s) 2025. CC BY 4.0 License.

A significant amount of explosive Mediterranean cyclones are located in the northwestern Mediterranean due to orographic deformation of the flow of baroclinic waves from the Atlantic generated by the Alps (Carniel et al., 2024). Moreover, Raveh-Rubin and Flaounas (2017) found in reanalysis data that the 200 most intense Mediterranean cyclones are often related to fast-intensifying cyclones in the Atlantic and are precursed by Rossby wave breaking. Also, cyclones associated with extreme wind speeds in the eastern Mediterranean are frequently located north of a jet streak related to the subtropical jet or a merging of the midlatitude and subtropical jet (Flaounas et al., 2015b; Raveh-Rubin and Wernli, 2015). Prezerakos et al. (2005) conducted a case study of an intense cyclone that caused heavy rain and winds in the eastern Mediterranean, which rapidly reintensified after entering the left exit region of the subtropical jet and the right entrance region of the midlatitude jet.

One big caveat using GCMs, is that the resolution is often too coarse to represent the complex topography of the Mediterranean and the generally smaller-scale cyclones and their dynamics within the Mediterranean (Flaounas et al., 2013). Hence, studying Mediterranean cyclones within high-resolution regional climate models (RCM) can be beneficial. For example, Chericoni et al. (2025) showed that the ability to reproduce higher moisture fluxes in their RCM with a 12 km horizontal resolution, lead to higher cyclone-related extreme precipitation. Thus, the purpose of this study is to investigate the impact of future climate change on extreme Mediterranean cyclones and their characteristics using a high-resolution RCM simulations. We utilize the Weather Research and Forecasting (WRF) model (Skamarock et al., 2021) to dynamically downscale the Community Earth System Model (CESM; Hurrell et al., 2013) simulation from 1821 to 2100 (Doensen et al., 2025) to a 20 km horizontal and a 1 hour temporal resolution. The analysis is focussed on wind, precipitation and compounding extreme cyclones (EXC) in the western and eastern Mediterranean. The future climate change signal is extracted by comparing the last 60 years of the 21st century under the representative concentration pathway (RCP) 8.5 conditions with the first 60 years of the simulation, representative for pre-industrial conditions.

This study is structured as follows. Section 2 describes the models, simulations and methods used. Section 3 presents the results, focussing on extreme precipitation, wind, and compounding cyclones. Then, we discuss the results in a broader context and end with final conclusions in Sect. 4.

2 Models, simulation and methods

2.1 Global and regional climate modelling

To quantify the behaviour of Mediterranean cyclones, we use a model chain from global to regional scales. The global model delivers the initial and boundary conditions for the regional model. The Community Earth System Model (CESM version 1.2.2; Hurrell et al., 2013) serves as global model. Kim et al. (2021) used this model to perform a late Holocene simulation, spanning 3600 years from 1500 BCE until 2100 CE (using the representative concentration pathway RCP8.5 scenario from 2012 to 2100). The output of this simulation has a temporal resolution of 6 hours and a spatial resolution of 1.9° (latitude) $\times$ 2.5° (longitude) in the atmosphere and over land, and a nominal $1.0° \times 1.0°$ resolution for the ocean and sea ice. The CESM simulation contains 30 vertical levels. In this study, we focus on the period from 1821 CE to 2100 CE (280 years) to capture both the pre-industrial and the future climate.

https://doi.org/10.5194/egusphere-2025-6315
Preprint. Discussion started: 28 December 2025
© Author(s) 2025. CC BY 4.0 License.

As RCM, we use the Weather Research and Forecasting (WRF) model version 4.3 (Skamarock et al., 2021) for dynamical downscaling. WRF is a mesoscale model that is based on the non-hydrostatic equations and a set of parameterizations to represent sub-grid-scale processes. We used the set of parameterization schemes listed in Table 1. For the Noah-MP land surface model, the phase change of glaciers is turned off, since this option causes numerical instabilities in our simulation.

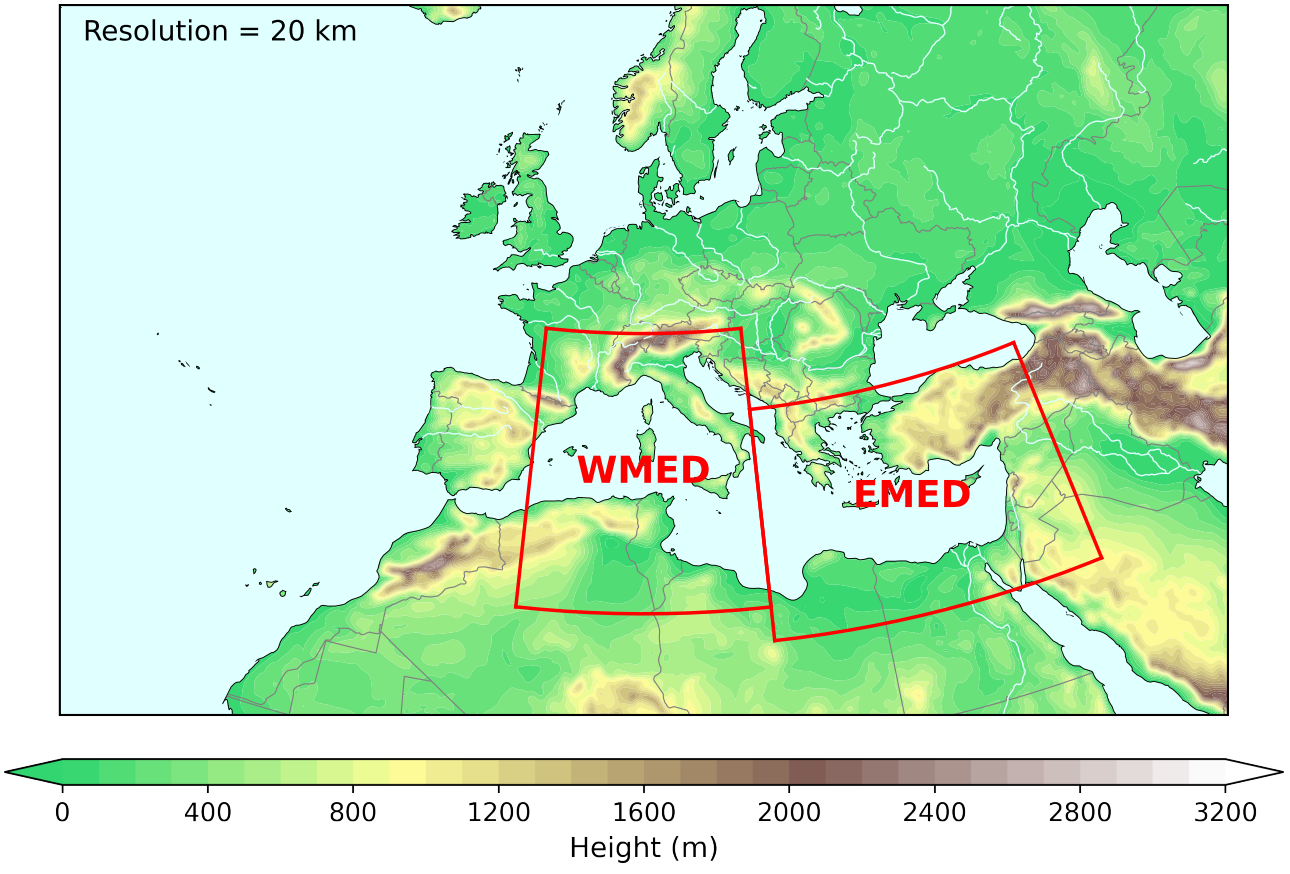

Figure 1. The domain used for the WRF simulation. The two subdomains used for the analysis are highlighted in red: Western (WMED) and eastern Mediterranean (EMED). Shading indicates the height of the model orography in meters above sea level using the WRF topography Global Multi-resolution Terrain Elevation Data (GMTED2010) provided by the United States Geological Survey (Danielson and Gesch, 2011).

95 The 280 years of the CESM simulation are dynamically downscaled to a horizontal resolution of 20 km and 49 vertical levels. A fixed time step of 120 s is used, and the data is stored with an hourly temporal resolution. To save time, we split up the 280 years in roughly 35 year chucks that always overlap for 2 years in time. The 2-year overlap is used as spin-up time for each chunk. Note that the land and atmosphere usually reach equilibrium after 6 to 12 months (Jerez et al., 2020). We use a single-domain setup covering the Euro-Atlantic area (Fig. 1). Nudging to the large scale circulation of the CESM simulation is

https://doi.org/10.5194/egusphere-2025-6315
Preprint. Discussion started: 28 December 2025
© Author(s) 2025. CC BY 4.0 License.

switched off, as the main cyclogenesis regions for Mediterranean cyclones are within this domain, and cyclones forming within this domain could develop their own dynamics independent of CESM input data. Although a horizontal resolution of 20 km is insufficient to numerically resolve convective processes, it is sufficient to accurately represent cloud-diabatic processes in fronts and conveyor belts that are crucial features in extratropical cyclones (Willison et al., 2013; Catto et al., 2019).

Table 1. Parameterization schemes used for the WRF simulation.

Parameterization scheme type	Parameterization scheme name
Microphysics	Thompson Scheme (Thompson et al., 2008)
Shortwave Radiation	Dudhia Shortwave Scheme (Dudhia, 1989)
Longwave Radiation	RRTM Longwave Scheme (Mlawer et al., 1997)
Surface Layer	Revised MM5 Scheme (Jiménez et al., 2012)
Land Surface	Noah–MP Land Surface Model (Niu et al., 2011) (without phase change of glaciers)
Planetary Boundary Layer	Yonsei University Scheme (YSU) (Hong et al., 2006)
Cumulus	Kain–Fritsch Scheme (Kain, 2004)

2.2 Cyclone tracking algorithm

Extratropical cyclones are tracked with the cyclone tracking algorithm developed by Blender et al. (1997), which is extended by Schneidereit et al. (2010) and Raible et al. (2018). It has been shown that this algorithm can represent cyclones realistically (Raible et al., 2008; Neu et al., 2013; Doensen et al., 2025).

The algorithm tracks minima in the geopotential height field, and we apply it to the hourly 850 hPa geopotential height (Z850) field in WRF. Since tracking cyclones in the lower atmosphere at higher resolution is difficult, because of noise introduced by the topography, we regrid the Z850 field of the WRF simulation to $1^\circ \times 1^\circ$ resolution (roughly 100 km). The regridding excludes weak and unphysical lows. Additionally, we apply a linear smoothing of all grid cells within 2° of one grid cell. With this, we prevent cyclone tracks from being split into multiple tracks. To further define cyclones, the following criteria of identified local minima must be met:

- A minimum mean gradient of at least 20 geopotential meters (gpm) per 1000 km.
- A minimum mean gradient of 75 gpm per 1000 km at least once during the lifetime of the cyclone.
- Local minima over grid cells with an orography higher than 1000 m above sea level are excluded.
- To connect all the minima of a cyclone track together, a minimum in the following time step is identified with a next-neighbour search. The new minimum of the cyclone one hour later had to be within roughly 40 km of the previous cyclone minimum.
- The minimal lifetime of a cyclone is at least 12 h.

https://doi.org/10.5194/egusphere-2025-6315
Preprint. Discussion started: 28 December 2025
© Author(s) 2025. CC BY 4.0 License.

Since the cyclones are tracked on the $1° \times 1°$ Z850 field, the location of the cyclones often does not match the actual Z850 minimum in the higher 20 km resolution data. Therefore, for every point within the cyclone track, we search for the actual Z850 minimum in the higher resolution Z850 field within a 100 km radius of the original cyclone track point. Next, we assume a cyclone radius of 500 km which corresponds to the average radius found for Mediterranean cyclones (Trigo et al., 1999).

2.3 Extreme cyclones

To focus on EXCs in the Mediterranean, we calculate the 95th-percentile precipitation and wind speed within the radius of 500 km. The time at which the cyclone reaches its minimum core sea level pressure is a good indicator of when the cyclone achieves its highest wind speeds (Pfahl and Sprenger, 2016) and for every cyclone track we assess 850 hPa wind speed (WS850) at this time step (t_{slp}). Peak precipitation in a cyclone often occurs a couple of hours before t_{slp} (Booth et al., 2018). Hence, for precipitation, we use the rolling summed 6 hourly 95$^{\text{th}}$-percentile precipitation within the 500 km radius, which is the sum of the precipitation 3 hours before and 2 hours after a specific time step ($precip_{6h}$). The time within the track, when $precip_{6h}$ is the highest, is defined as t_{precip}. Next, EXC extremeness is measured by how many standard deviations WS850 at t_{slp} and $precip_{6h}$ at t_{precip} deviate from the mean 95th-percentile precipitation and wind speed across all tracked cyclones over the whole 280-year period. Since $precip_{6h}$ data are typically highly skewed, we use a power-law transformation to make the $precip_{6h}$ distribution more Gaussian. Specifically, the two-thirds power transformation is used, which is equivalent to taking the cube root of the squared $precip_{6h}$ data. For compounding events, we compute the joint probability distribution of the precipitation and wind speed EXCs and ranked their extremeness based on the joined distribution.

2.4 Definition of regions and study periods

To highlight the climatological differences within the Mediterranean, we split up the Mediterranean into two regions (two red boxes in Fig. 1), namely the western Mediterranean ("WMED", between 0° E - 17.5° E and 30° N - 47° N), and the eastern Mediterranean ("EMED", between 17.5° E - 40° E and 28° N - 42° N). All analyses are performed for each region separately.

To assess the effect of climate change on Mediterranean cyclones, we use two 60-year periods. The first period is defined as all winter half-years (ONDJFM) starting in October 1821 until March 1881 and roughly representing the pre-industrial climate. The second period is defined as all winter half-years from October 2039 until March 2099 representing the future climate under the RCP8.5 scenario. These periods and the EXCs within these periods will be referred to as *past* and *future*, respectively.

We apply a Kolmogorov-Smirnov (KS) test (An, 1933) in the analyses to test statistical significnace at the 5 % level. For location, we use KS test to see if the median latitude and longitude of the future EXC changes. For the climatology, we use the KS test whether future EXCs occurred at different times, by assessing if the median day-of-year of each EXC type changed in each region.

https://doi.org/10.5194/egusphere-2025-6315
Preprint. Discussion started: 28 December 2025
© Author(s) 2025. CC BY 4.0 License.

2.5 Composite analysis

Finally, a cyclone-centred composite analysis is performed on the 50 most extreme EXCs found in the WMED and EMED, respectively. This number roughly corresponds to the 5% most extreme cyclones found for each region in the past and the future. The analysis is performed for cyclones associated with cyclone-related precipitation, wind, and compound extremes, separately.

1. For each cyclone track, we set the reference at time t_{slp} or t_{precip} for wind speed EXCs and precipitation EXCs, respectively. Every time step of the track after t_{slp} or t_{precip} receives a positive index, and the time steps of the track before t_{slp} or t_{precip} a negative index.

2. For each of the hourly time steps of the cyclone track, all fields are centred at the location of the cyclone, given by its core minimum Z850. With this approach, the model data for each cyclone track point is independent of its geographical location.

3. We are only interested in the 12 hours before and after t_{slp} or t_{precip} for each cyclone to capture the intensification and decaying phase of the cyclone.

4. Within this time period, we compute spatial averages from the 50 most extreme EXCs.

We perform the above analysis for the WS850, $precip_{6h}$, and the 200 hPa wind speed (WS200) field. Note that some EXC tracks may initialize later than 12 hours before t_{slp} or t_{precip}, and may also disappear earlier than 12 hours after t_{slp} or t_{precip}. Hence, the composites shown at 12 hours before and after t_{precip} or t_{slp} consists of slightly less than 50 EXCs. To compute whether the differences in spatial means for past and future cyclones is statistically significant we apply a Welch's t-test (Welch, 1947) to the spatial composite.

Furthermore, we also compute vertical cross-sections for the 50 most extreme precipitation EXCs, where we vertically interpolated on 21 pressure levels an east-west plane through the cyclone core spanning 1600 km in total. For these vertical cross-sections, we computed anomalies, potential temperature (θ) and equivalent potential temperature (θ_e) for 21 pressure levels up to 100 hPa (50 hPa intervals from 100 to 900 hPa and 25 hPa intervals from 900 to 1000 hPa). PV anomalies were computed by subtracting the daily PV climatology, calculated separately for the past and future period, from the instantaneous PV fields. The climatology was derived by averaging PV for each calendar day and applying a centred 31-day running mean.

3 Results

3.1 Climatology of mean and extreme cyclones

Here, we characterize the preferred regions of all and extreme cyclones in the Mediterranean. Therefore, we use the cyclone frequency, defined by how often a grid cell is within the radius of a cyclone (defined as 500 km) in the original WRF grid.

https://doi.org/10.5194/egusphere-2025-6315
Preprint. Discussion started: 28 December 2025
© Author(s) 2025. CC BY 4.0 License.

Enhanced mean cyclone frequency is consistently found in a band spanning from the Tyrrhenian Sea to the Levant with maxima over Italy and northern Greece to the Anatolian Plateau (Fig. 2). These regions exhibit the highest cyclone frequencies in both the past (up to 0.09 cyclones day^{-1}; Fig. 2a) and the future (up to 0.07 cyclones day^{-1}; Fig. 2b). Comparing the future with the past period, a decrease in cyclone frequency is evident (Fig. 2c). Apart from a few regions in northern Africa, all regions in the Mediterranean show a decline in mean cyclone frequency. This is especially the case over the maxima in Italy and the Anatolian Plateau, which show the largest absolute decrease in cyclone frequency (up to 0.02 cyclones day^{-1}), which in relative terms indicates a decrease of roughly one-third.

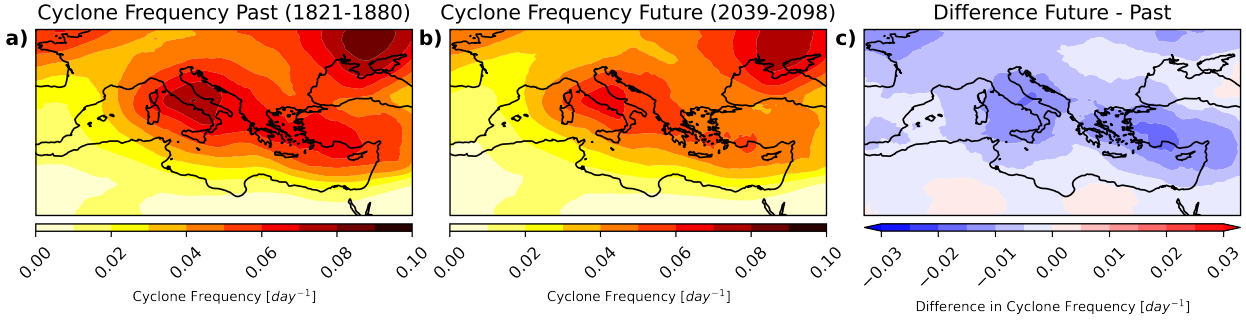

Figure 2. Mean cyclone frequency in the Mediterranean for the past (a; 1821-1880), the future (b; 2039-2098) and the absolute difference between the future and the past (c). Shading shows the number of times (day^{-1}) where a grid cell is within the 500 km radius around a cyclone centre.

Concerning extreme cyclones, we show the location of the 50 most extreme past and future EXCs for each region and each category at t_{slp} (Fig. 3). In the WMED (Fig. 3a–c), wind speed EXCs are distributed over the entire domain, whereas precipitation and compound EXCs cluster over the warm waters of the Tyrrhenian and Adriatic Sea, and over Northern Italy. Future precipitation EXCs in the WMED (Fig. 3b) seem to occur less often over the Mediterranean and Ligurian Sea. In the EMED (Fig. 3d–f), all EXC types tend to cluster in the Ionian and Aegean Sea, and over northern Greece and the Anatolian Plateau. Future precipitation and compound EXCs (Fig. 3e and 3f) tend to be located more over the Mediterranean Sea south of Turkey.

https://doi.org/10.5194/egusphere-2025-6315
Preprint. Discussion started: 28 December 2025
© Author(s) 2025. CC BY 4.0 License.

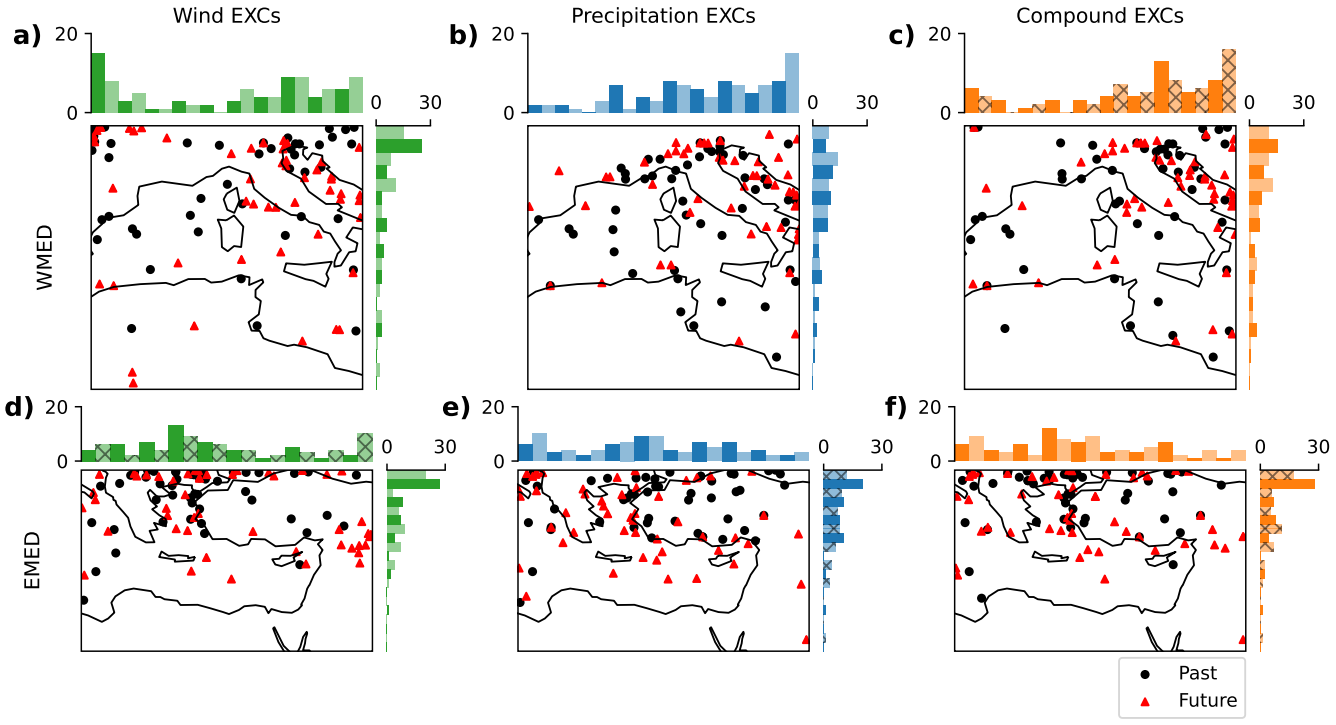

Figure 3. Location of 50 most extreme EXCs in WMED (a–c), and EMED (d–f). Shown are locations of wind EXCs (left column), precipitation EXCs (middle column), and compound EXCs (right column). Black circles indicate past EXC, red triangles indicate future EXCs. The bars indicate the number of cyclones binned in groups 10 for each longitude and latitude. Green, blue and orange bars indicate wind, precipitation and compounding EXCs, respectively. The lighter shaded bars indicate past EXCs, whereas darker shaded bars indicate future EXCs. Hatched bars indicate a statistically significant change (5% level) in longitude or latitude.

For each subpanel, we also show histograms of the longitudes and latitudes (Fig. 3) to investigate whether the median location of EXCs changes as a result of climate change. Indeed, the southward shift of precipitation and compound EXCs in the EMED in the future is statistically significant at the 5% level. We also find a significant eastward shift of compound EXCs in the WMED in the future (Fig. 3c), and of wind EXCs in the EMED (Fig. 3d). The latter is most likely caused by the future cluster popping up in the Levant.

Besides the spatial changes, we investigated also changes in the monthly occurrence of extreme cyclones during the extended winter season. In Fig. 4, we show the number of EXCs that occur every month of the winter half-year for the WMED and EMED in the past and the future. Wind and compounding EXCs are distributed evenly over the entire winter half-year. Still, wind EXCs occur more frequently in the second and colder part of the winter half year, whereas compounding EXCs tend to be more frequent during the first part of the winter half-year. The occurrence of precipitation EXCs (blue bars) peaks in autumn when the Mediterranean Sea is still warm and evaporation from the sea surface can nourish precipitation of the cyclone, and these cyclones hardly occur in the second part of the winter half-year for both regions. This decrease is very abrupt in the

https://doi.org/10.5194/egusphere-2025-6315
Preprint. Discussion started: 28 December 2025
© Author(s) 2025. CC BY 4.0 License.

central Mediterranean (Fig. 4a), whereas in the eastern Mediterranean it is more gradual (Fig. 4b). Comparing the past with the future distributions during the extended winter, we do not find a statistically significant impact on the median t ime of occurrence of EXCs. Thus, the seasonality of extreme cyclones remains unchanged under future RCP8.5 conditions.

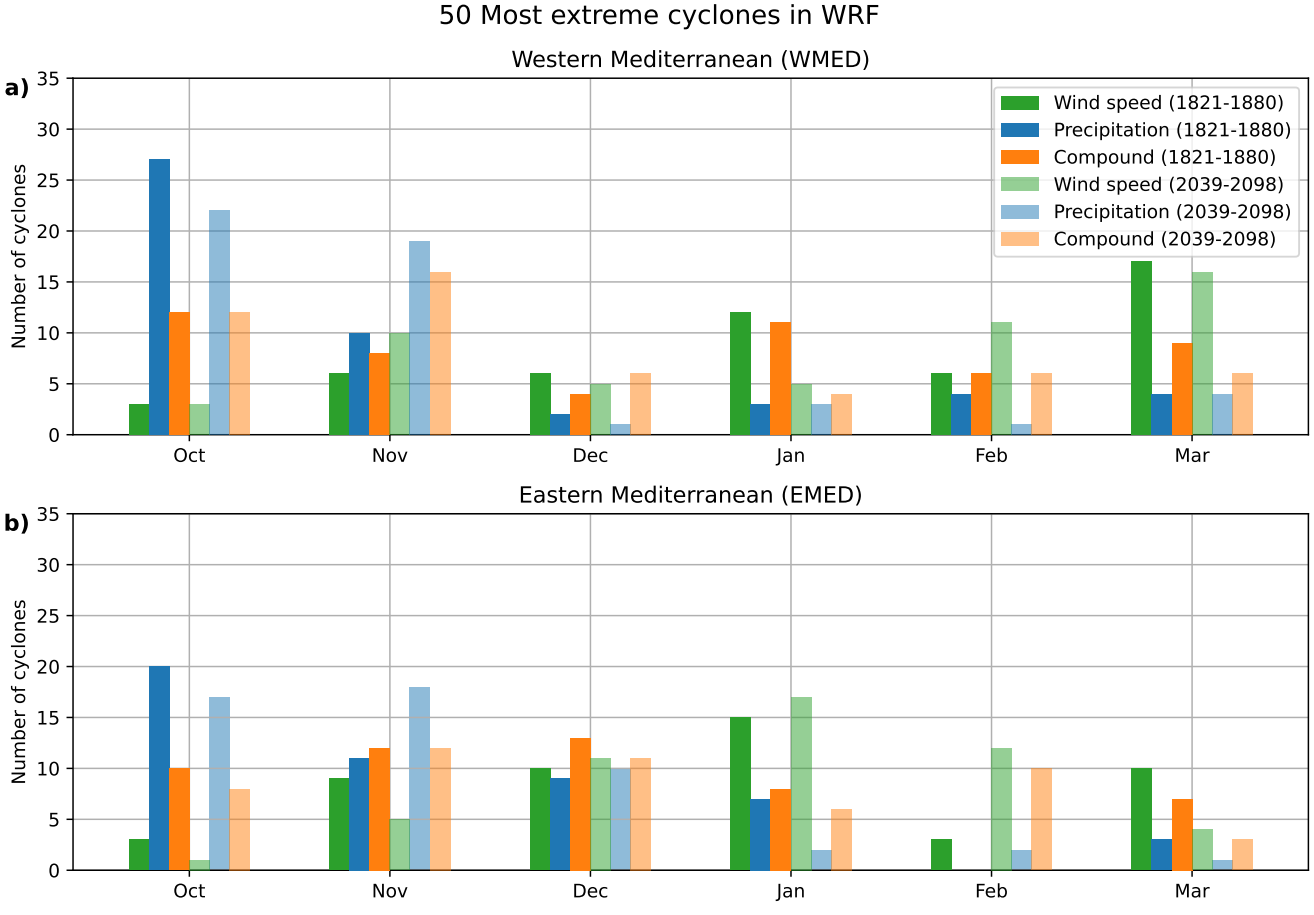

Figure 4. Number of Mediterranean EXCs per month in the WMED (a) and EMED (b). Green, blue and orange bars show the number of wind, precipitation and compounding EXCs, respectively. Plain bars indicate the number of EXCs in the past (1821–1880), and semi-transparent coloured bars indicate the number of EXCs in the future (2039–2098).

3.2 Cyclones associated with extreme precipitation

Here, we assess the life cycle of the precipitation EXCs using the composite analysis. In Fig. 5, the 50 most extreme precipitation EXCs are shown for the WMED and EMED, assessing past and future EXCs before, at and after their most intense precipitation phase t_{precip}. In all composites, we see the general structure of a cyclone with a clear minimum in sea level pressure and precipitation bands north and southeast of the EXC center.

https://doi.org/10.5194/egusphere-2025-6315
Preprint. Discussion started: 28 December 2025
© Author(s) 2025. CC BY 4.0 License.

We start with the life cycle of past precipitation EXCs (Fig. 5a-c and j-l). 12 hours before t_{precip} (left column) the highest precipitation is observed mostly north of the EXC centre in both regions, with the most intense precipitation found very close to the EXC center (Fig. 5a,j). In the EMED, a precipitation band southeast of the EXC center is visible, possibly indicating the development of frontal structures (Fig. 5j). At t_{precip} (Fig. 5b,k), precipitation further intensifies and the development of potential frontal structures is evident. Highest precipitation is still observed just north of the EXC centre, with precipitation rates up to and exceeding 25 mm 6h^{-1} for past and future (Fig. 5b) EXCs in the WMED respectively. In the composites 12 hours after t_{precip}, precipitation rates significantly decrease in both regions (Fig. 5c,l). Close to the EXC center, precipitation rates have fallen the most (in the order of 10 to 15 mm 6h^{-1}). Nevertheless, frontal structures are still recognizable in both regions 12 hours after t_{precip}. The life cycle of precipitation goes along a general intensification of the pressure field. The core pressure of precipitation EXCs falls by 5 hPa comparing the composites at $t_{precip}$with 12 hours before t_{precip}. 12 hours after t_{precip}, the core pressure is still relatively low, which is most likely due to the fact that precipitation peaks before core pressure reaches its minimum.

https://doi.org/10.5194/egusphere-2025-6315
Preprint. Discussion started: 28 December 2025
© Author(s) 2025. CC BY 4.0 License.

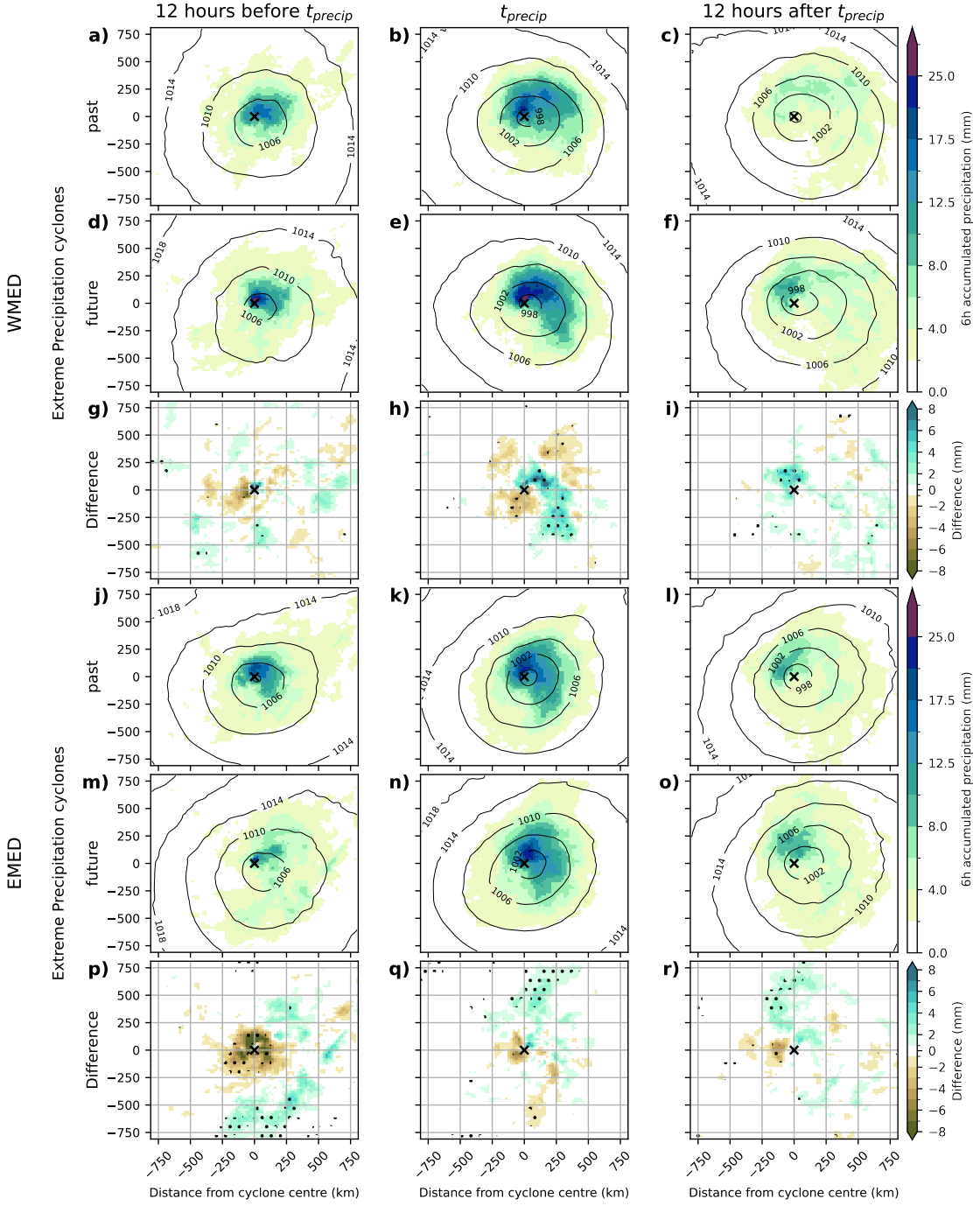

Figure 5. A composite of the 50 most extreme precipitation EXCs in the WMED (a–i) and EMED (j–r) showing $precip_{6h}$. Panels a–c and j–l show composites for the past (1821–1880), panels d–f and m–o show composites for the future (2039–2098), and panels g–i and p–r show the differences between the past and future, where stippling indicates that differences are statistically significant (5% level). Shading indicates mean summed 6-hourly precipitation, and contour lines indicate the mean sea level pressure. The left column shows composites 12 hours before t_{precip}, the middle column at t_{precip} and the right column 12 hours after t_{precip}.

https://doi.org/10.5194/egusphere-2025-6315
Preprint. Discussion started: 28 December 2025
© Author(s) 2025. CC BY 4.0 License.

The life cycle of future precipitation EXCs show a similar intensification of precipitation and core pressure for both regions (Fig. 5d–f and m–o). To illustrate the climate change signal in the life cycle, we focus on the difference between past and future EXCs in both regions (Fig. 5g–i and p–r). First, looking at the composites 12 hours before t_{precip}, we see a considerable decrease in precipitation for future precipitation EXCs around the EXC center in both regions. In the WMED, the decrease around the core is rather minor, and not significant (Fig. 5g). In the EMED (Fig. 5p) the decrease in precipitation reaches up to 8 mm 6h^{-1}, i.e., a decrease of almost half. Notably, precipitation increases significantly further away from the EXC center in the EMED. The reduction in precipitation is less apparent at mature state at t_{precip}. For precipitation EXCs in the WMED (Fig. 5h), a dipole pattern forms with a significant increase in precipitation just north of the EXC center and within the fronts (southeast of the EXC center), and a significant decrease in precipitation just south of the EXC center. The areas where the precipitation increases overlap with the areas where precipitation is most intense already (Fig. 5b and 5e), hence indicating an increase in the impact of future precipitation EXCs at t_{precip} in the WMED. In the EMED, a general decrease in precipitation is still apparent around the core at t_{precip} (Fig. 5q), although its magnitude is smaller and the signal does not reach statistical significance. Interestingly, the precipitation increase that occurs south of the EXCs in Fig. 5p disappears, and a precipitation increase north of the EXCs appears. Thus, the results suggest that at t_{precip}, WMED EXCs tend to produce more and EMED EXCs tend to produce roughly the same amount of precipitation. This difference further amplifies in the composites 12 hours after t_{precip}. In the WMED, we find a significant increase in precipitation north of the EXC center in the order of 5 mm 6h^{-1} (Fig. 5i). This is a doubling compared to past precipitation EXCs (Fig. 5c).

At 12 hours before t_{precip}, future extreme precipitation EXCs tend to be slightly less deep in terms of core pressure compared to past precipitation EXCs in both the WMED and the EMED. This suggests that future EXCs are less intense with respect to pressure before their mature stage, providing a partial answer to why future precipitation rates are less overall compared to the past in both regions. At t_{precip}, precipitation EXCs are equally deep for the past and future in the WMED where future precipitation EXCs have overcome a slightly larger core pressure difference compared to past cyclones (Fig. 5a–b vs. Fig. 5d–e). In the meantime, the higher core pressure for future precipitation EXCs persists in the EMED (Fig. 5k vs. Fig. 5n). This partly explains why extreme precipitation in the WMED somewhat increases, in contrast to the EMED. 12 hours after t_{precip}, the difference in core pressure between the WMED and EMED persists.

To further explain why future precipitation WMED EXCs tend to be stronger in their mature phase, we show vertical cross-sections of PV anomalies, potential temperature (θ) and equivalent potential temperature (θ_e) within the composites of Fig. 5. We focus on 6, 9 and 12 hours after t_{precip}, as differences in PV between past and future EXCs only start to emerge in the mature phase of the cyclone.

https://doi.org/10.5194/egusphere-2025-6315
Preprint. Discussion started: 28 December 2025
© Author(s) 2025. CC BY 4.0 License.

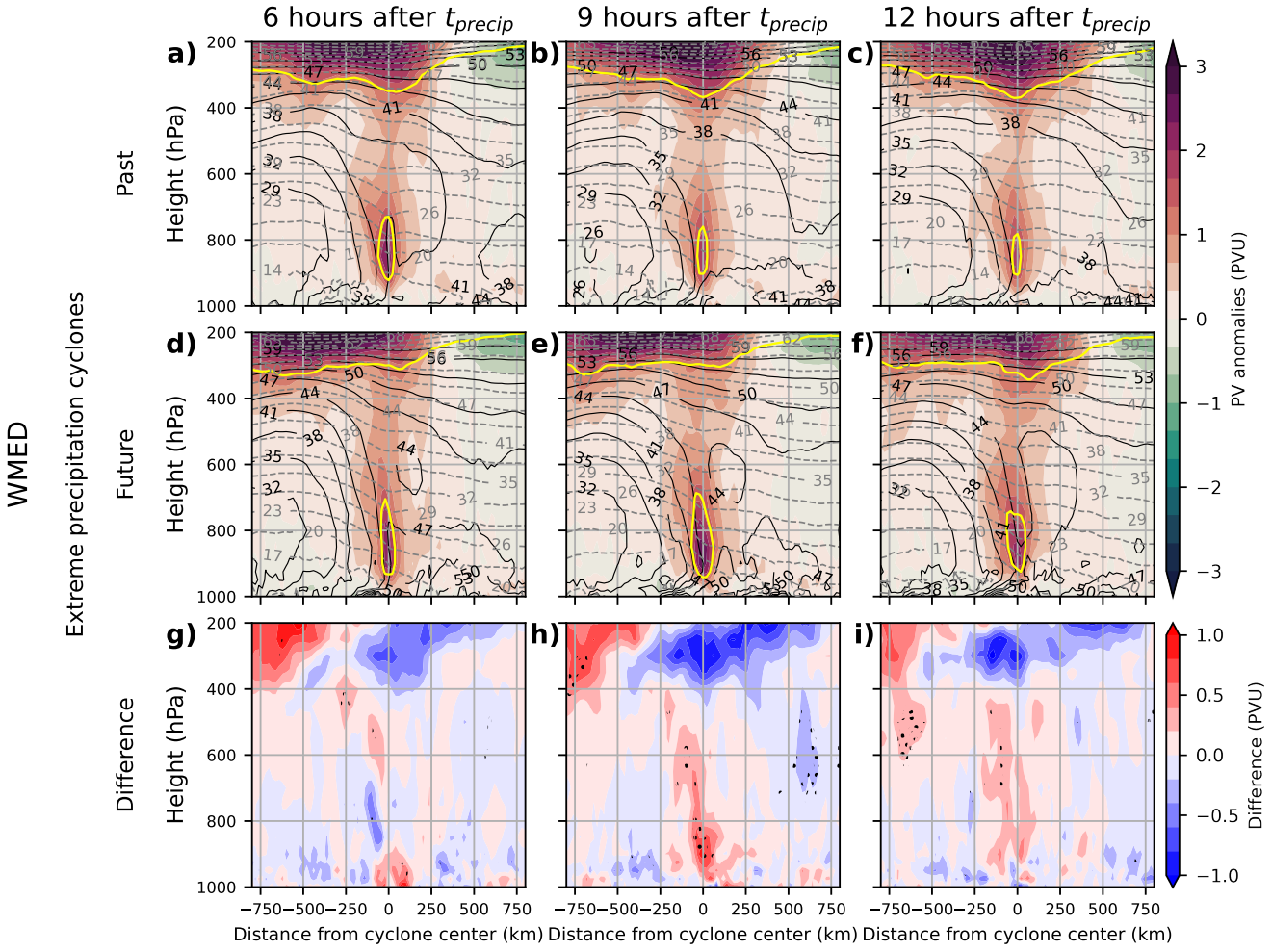

Figure 6. Vertical cross section of WMED precipitation EXCs but ranging from 800 km west to 800 km east of the EXC centre, right through the EXC centre. Shading shows PV anomalies [PVU], continuous contour lines show equivalent potential temperature (θ_e) [°C] and dashed contour lines show potential temperature (θ) [°C]. Shown are past precipitation EXCs (a–c), future precipitation EXCs (d–f) and the difference between the future and past for 6 (left column), 9 (middle column) and 12 hours (right column) after t_{precip} . Stippling indicates a statistically significant difference (5% level). The yellow line indicates the 2 PVU contour of instantaneous PV.

In all sub-panels of Fig. 6, we find higher values of θ and θ_e in the right half of the vertical cross sections and lower values in the left half, highlighting the warm and cold sector of the EXCs, respectively. In the warm sector, θ and θ_e diverge more strongly than in the cold sector, indicating the abundance of moisture. Besides, the negative vertical gradients in θ_e in the lower part of the troposphere (e.g. in the right-hand side of Fig. 6e) points to convective instability. Both θ and θ_e increase for future EXCs (Fig. 6a–c) vs. Fig. 6d–f), but θ_e in the warm sector increases up to 9 °C, showing a combined increase in temperature and moisture in the atmosphere in the future, which further explains the increase in precipitation of EXCs in WMED.

https://doi.org/10.5194/egusphere-2025-6315
Preprint. Discussion started: 28 December 2025
© Author(s) 2025. CC BY 4.0 License.

Looking at PV anomalies, we also find future changes in its vertical structure (Fig. 6). In all composites around 300 hPa, we identify high PV air in excess of 2 PVU (indicated by the yellow line) indicating the stratosphere air masses. The high PV anomalies above the yellow line indicate a lowering of the tropopause in the vicinity of precipitation EXC. This is in contrast to the upper atmosphere east of the cyclone centre, which is dominated by negative PV anomalies indicating a higher than usual tropopause. Additionally, so-called PV towers with high PV anomalies are present near the cyclone centre (Fig. 6). These PV towers consist of high-PV stratospheric air intruding into the top of the PV tower, and diabatically produced PV in the lower troposphere. These PV towers exhibit sufficiently large potential vorticity air masses such that the 2 PVU line even becomes visible in all composites. Generally we see the same structures also for precipitation EXCs in the EMED (Fig. S3a–f).

When looking at the future differences in Fig. 6g–i, we see a general decrease of PV near the tropopause in the warm sector, indicating the lifting of the tropopause in general. In the cold sector, PV increases near the tropopause, which indicates stronger PV advection from the stratosphere and is also indicative of a more intense baroclinic cyclone. Interpretations should be taken with care, though, as the changes observed near the tropopause are not or barely statistically significant (at the 5% level). Still, it should be noted that we do not see this enhanced advection of high PV air for precipitation EXCs in the EMED (Fig. S3g–i). Generally, the PV values within the PV tower increase for future precipitation EXCs (Fig. 6g–i). This is especially the case at 9 hours and to a lesser extent at 12 hours after t_{precip} (Fig. 6h and Fig. 6i) with increases up to 1 PVU. Although the increase is statistically not very robust, this still indicates an increase of up to 50% in instantaneous PV in Fig. 6h. This is most likely due to an increase in diabatically produced low-level PV as a result of more moisture and hence higher condensation for future WMED precipitation EXCs. This may enhance the cyclonic circulation and provide a mechanism of why future WMED precipitation EXCs exhibit a stronger intensification and stay more intense in their mature phase. We also see an increase of PV in the PV towers associated with future precipitation EXCs in the EMED, but this increase is clearly less robust (Fig. S3g–i).

3.3 Cyclones associated with wind extremes

In this section, we investigate the life cycle of the wind EXCs, following a similar strategy as for precipitation EXCs. Using again the composite analysis of the 50 most extreme events (Fig. 7), we find that the highest wind speeds are generally located just south or southeast of the EXC center with WS850 values of up to 25 ms^{-1}. Minimum core pressure falls below 990 hPa in most composites, and core pressures are generally up to 10 hPa lower than for precipitation EXCs with higher pressure gradients as well.

The development of the past wind EXCs and the associated wind field is shown in Fig. 7a–c and j–l. At 12 hours before t_{slp} (left column), the wind EXCs already deepened substantially, and the wind field is strongest south and southeast of the core. EXCs in the WMED (Fig. 7a and 7d) tend to be slightly deeper and more intense than EXCs in the EMED (Fig. 7j and 7m). At t_{slp} (middle column), the wind EXCs has deepened around 4 hPa in all composites. The wind field has clearly intensified and expanded, especially in the EMED. EXCs in the WMED are slightly deeper than in the EMED (roughly 4 hPa), and achieve higher wind speeds in the EMED. A striking difference between the two regions is that EXCs in the EMED have a much more southwest-northeast orientation than in the WMED. 12 hours after t_{slp} (right column), the core pressure of the EXC has increased slightly, and the wind field has shrunk in size and intensity substantially. We also see a general shift of the

https://doi.org/10.5194/egusphere-2025-6315
Preprint. Discussion started: 28 December 2025
© Author(s) 2025. CC BY 4.0 License.

remaining wind field towards the east relative to the EXC centre compared to the composites 12 hours before t_{slp}, especially in the WMED. The wind field in the EMED (Fig. 7l and 7o), is slightly stronger than the wind field in the WMED (Fig. 7c and 7f) by about 2-3 ms^{-1} at t_{slp}.

https://doi.org/10.5194/egusphere-2025-6315
Preprint. Discussion started: 28 December 2025
© Author(s) 2025. CC BY 4.0 License.

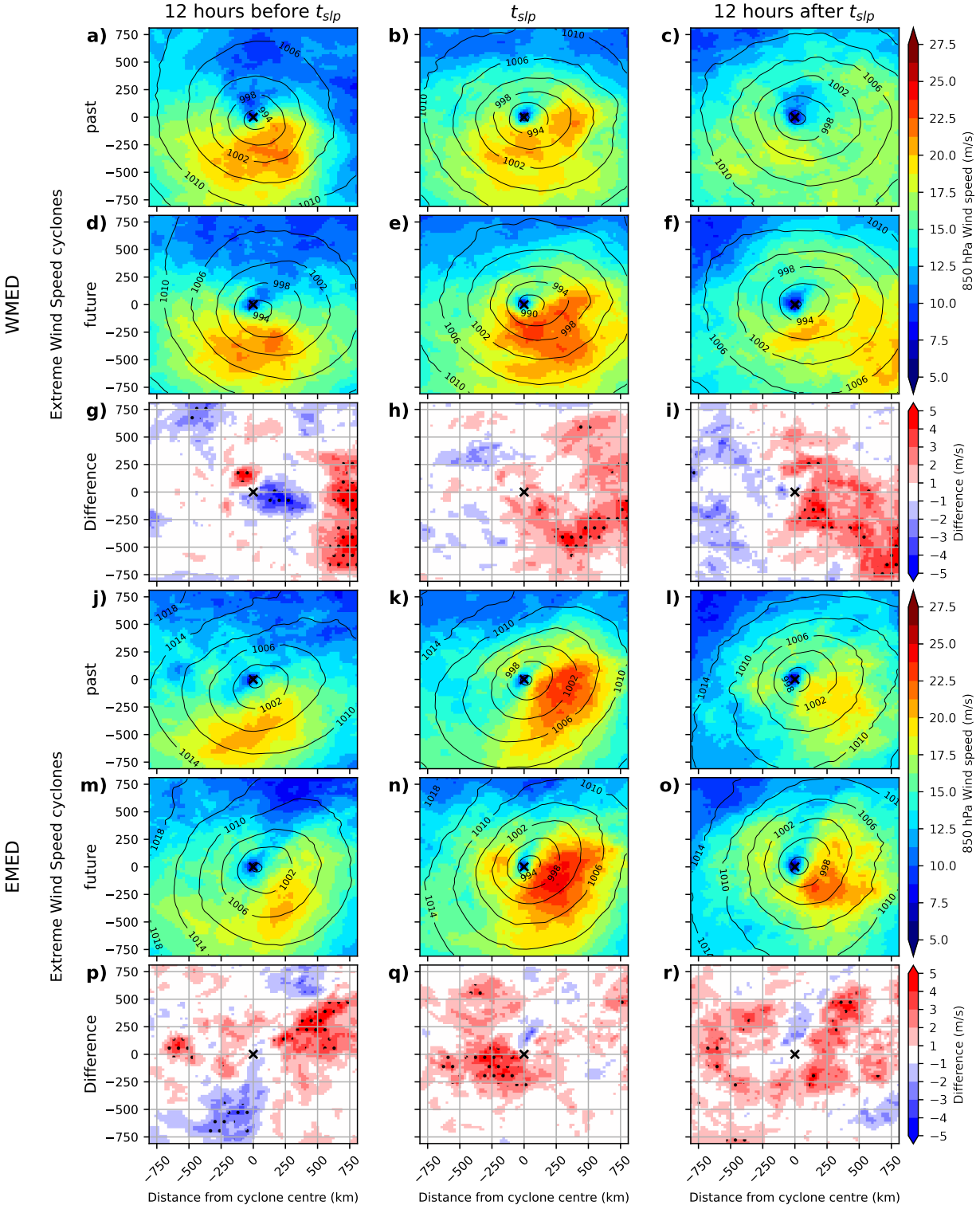

Figure 7. Same as Fig. 5, but now for 850 hPa wind speed. The left column now indicates 12 hours before t_{slp}, the middle column at t_{slp}, and the right columns 12 hours after t_{slp}.

https://doi.org/10.5194/egusphere-2025-6315
Preprint. Discussion started: 28 December 2025
© Author(s) 2025. CC BY 4.0 License.

The life cycle of future wind EXCs intensifies in a similar way as the one of past wind EXCs (Fig. Fig. 7). To extract the future climate change signal, we show the difference between the past and the future (Fig. 7g–i and p–r). 12 hours before t_{slp} (left column), in the WMED (Fig. 7g) we find a complex pattern of WS850 changes near the EXC center, with opposing anomalies largely offsetting each other. 750 km east of the EXC center, the wind speed is signifcantly increased by up to 4 ms^{-1} in the future. In the EMED, we also find a complex pattern in wind speed differences between the past and future (Fig. 7p) which is different to the WMED. The EMED wind cyclones show an increase in wind speed west and east of the cyclone core and a decrease south of the cyclone core. This is mainly due to differences in wind field orientation, as the analysis of the shape of past and future EXCs (Fig. 7j,m) suggests.

At t_{slp} (middle column), we see a more uniform pattern in wind speed differences. In the WMED, a general increase in wind speed appears (Fig. 7h), with a significant increase in wind speed in the southeastern quadrant of the composite, which is also the quadrant with the highest wind speeds overall. Only in the western half of the EXC do we observe a slight decrease in wind speed, but this decrease is not statistically significant. Unlike the WMED, in the EMED we observe a statistically significant increase in wind speed in the western half of the EXC composite (Fig. 7q). Comparing the shape of the wind field between past and future EXCs (Fig. 7k,n), this increase is mainly induced by a small wind field just west of the core for future EXCs. Apart from that, the wind fields stay similar in size and intensity.

At 12 hours after t_{slp} (right column), the difference patterns are similar to the ones at t_{slp}. Again, we see a statistically significant increase in wind speed in the southeastern quadrant of the WMED EXCs and a non-significant decrease in the western half of the WMED EXCs (Fig. 7i). In the EMED, we see a significant increase just south of the EXC center (Fig. 7r). Note that the magnitude of these differences is equal to the ones at t_{slp} (Fig.7h and 7q) but occur at lower overall wind speeds, so the relative difference between past and future EXCs 12 hours after t_{slp} is greater compared to t_{slp}.

At 12 hours before t_{slp}, past and future EXCs in both regions have roughly the same core pressure. At t_{slp}, future cyclones deepen more and core pressure for EXCs in both regions is lower than for past cyclones. This difference persists 12 hours after t_{slp}, where the differences in core pressure increase even further. This provides a partial explanation of why wind speed EXCs appear stronger in their mature phase.

To further understand why wind EXCs in the future tend to be stronger in their most intense and mature phase, we investigate the jet stream as a potential driver. In Fig. 8, we apply the same composite analysis as in Fig. 7, but now to wind speed at 200 hPa (WS200). With this, we characterize the strength and location of the jet stream relative to the wind EXCs. The analysis shows that WS200 values are generally the highest about 1000 km south of the EXC center, indicating that the EXCs are usually located on the northern edge of the jet. Furthermore, another branch of high WS200 values is present west of the EXC centre, especially 12 hours before t_{slp} and at t_{slp}. This is a hint that a branch of the polar jet merges with the subtropical jet. Generally, WS200 values are much higher in the EMED (exceeding 60 ms^{-1}) compared to the WMED (up to 50 ms^{-1}). A likely explanation for this is the more southern location of the EMED region (Fig. 3) and hence EXCs tend to be located closer to the subtropical jet.

Considering all composites, a jet speed maximum is positioned just south of the EXC centre, indicating a jet streak. At 12 hours before t_{slp}, the EXC is located right above the jet streak maximum, where potential effects of the jet stream neither aid

https://doi.org/10.5194/egusphere-2025-6315
Preprint. Discussion started: 28 December 2025
© Author(s) 2025. CC BY 4.0 License.

nor inhibit the development of the EXC. At t_{slp}, the EXC moves towards the left exit of the jet streak, which is the region where upper air divergence leads to rising air motions and hence can prolong EXC intensity in its mature face. At 12 hours after t_{slp}, the EXC has moved further east relative to the jet streak and is now positioned clearly in the left-exit region of the jet streak. This behaviour is especially evident for wind EXCs in the EMED (Fig. 7j–o).

https://doi.org/10.5194/egusphere-2025-6315
Preprint. Discussion started: 28 December 2025
© Author(s) 2025. CC BY 4.0 License.

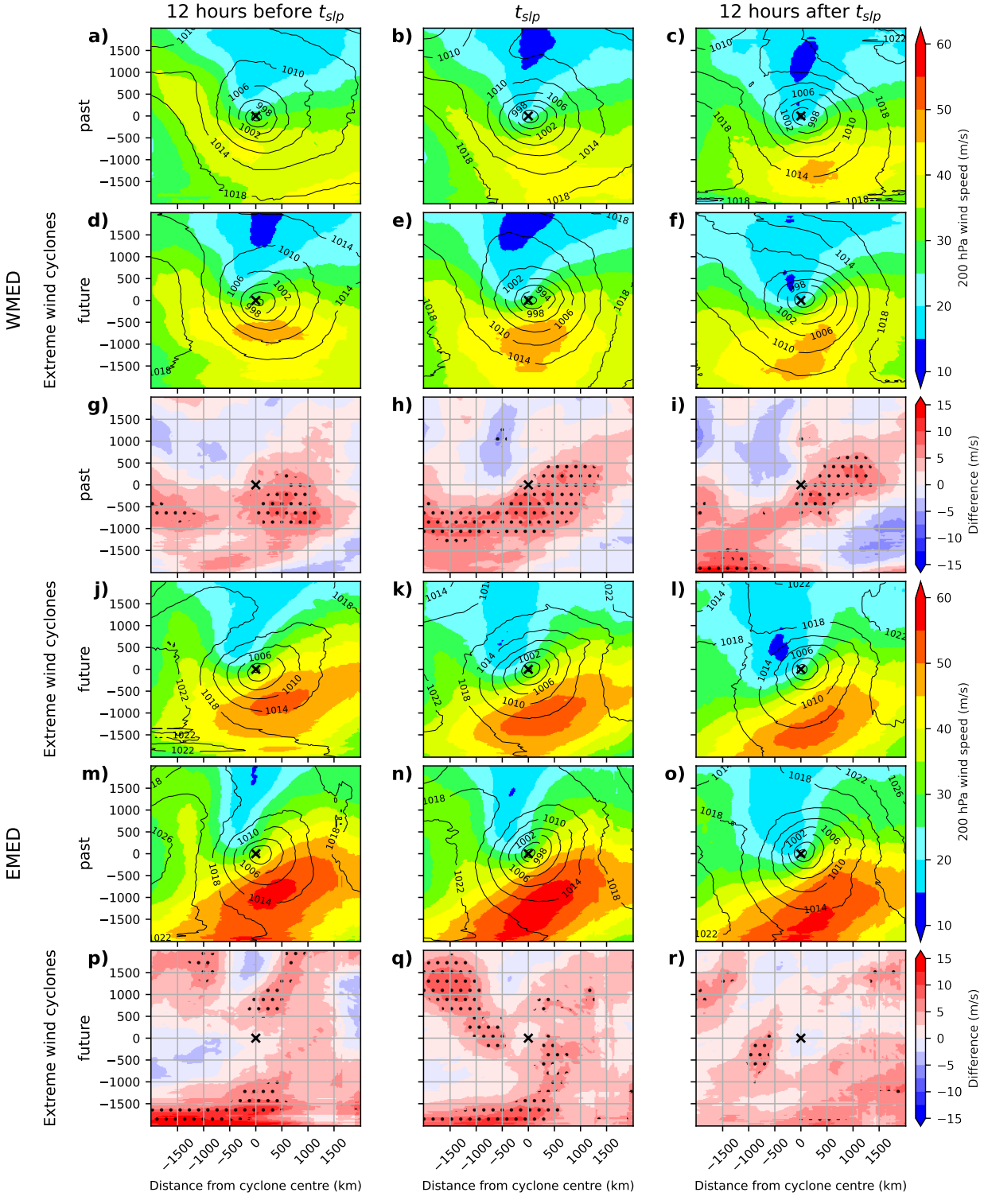

Figure 8. Same as Fig. 7, but now for 200 hPa wind speed. Note that the area away from the centre of the composites has expanded from 750 km to 2000 km.

https://doi.org/10.5194/egusphere-2025-6315
Preprint. Discussion started: 28 December 2025
© Author(s) 2025. CC BY 4.0 License.

Considering WS200 related to future Wind EXCs in the WMED Fig. 7g–i, we see a general increase in WS200 for both regions at all time steps. Consequentially, for wind speed EXCs in the WMED the jet streak appears at all time steps in the future (Fig. 8d–f) in contrast to the past (Fig. 8a–c). The jet streak maximum wind speed is up to 10 ms^{-1} higher compared to the past wind EXCs in the WMED and mostly statistically significant across all time steps (Fig. 8g–i). This eventually leads to a future EXC that is located in the left exit of a stronger jet streak in its mature phase (Fig. 8e–f).

In the EMED, we also identify an increase in WS200 within the jet stream across all time steps in Fig. 8p–r of up to 10 ms^{-1}. In this region, we also see a significant increase in WS200 northwest of the EXC center, indicating an increase in strength of the polar jet, especially at t_{slp} (Fig. 8q). Despite the increase in WS200 south of the EXC center (resembling the merged polar and subtropical jet), this increase is only significant at t_{slp} (Fig. 8q). Nevertheless, we also find future mature wind speed EXCs in the EMED in the left exit of a partially stronger jet streak. This means that future EXCs would also benefit from stronger rising air motions and could thus stay more extreme and sustain high wind speeds in EXCs.

3.4 Cyclones associated with compound precipitation and wind extremes

Lastly, we investigate the life cycle of precipitation and wind speed in compounding EXCs. For precipitation within compounding EXCs (Fig. S1), we largely see the same patterns as for precipitation EXCs (Fig. 5). Precipitation increases as the cyclone intensifies and decreases strongly again in its mature stage. Precipitation is slightly less intense than for precipitation EXCs and compounding EXCs have a lower core pressure (in the order of 4 hPa) to accommodate higher wind speeds. Also, future changes for compound EXCs are very similar to precipitation EXCs. However, compound EXCs in the EMED tend to get even drier than precipitation EXCs in the future (Fig. S1p–r).

Wind speeds in compounding EXCs (Fig. S2) are of similar intensity at t_{slp}compared to wind speed EXCs in Fig. 7. The wind field is of slightly smaller size though. 12 hours before t_{slp}, wind speeds of compounding EXCs are slightly lower compared to wind speed EXCs in both regions (left column of Fig. S2). 12 hours after t_{slp}, EMED compounding EXCs are significantly less intense than EMED wind speed EXCs, but of similar intensity in the WMED (left column of Fig. S2). Compound EXC core pressure is very similar to wind speed EXCs at t_{slp} and 12 hours after t_{slp}, but slightly higher 12 hours before t_{slp}. The increase in WS850 in future compound EXCs is slightly less in the WMED as compared to wind speed EXCs in the WMED (Fig. S2g–i). However, for compound EXCs in the EMED we see a large future decrease in wind speed (Fig. S2p–r), which is almost contrary to what we observe for future wind speed EXCs (Fig. 7p–r).

4 Discussion and conclusion

The aim of this study is to assess changes in wind, precipitation and compounding extreme cyclone characteristics in the Mediterranean by comparing pre-industrial with future conditions under RCP8.5. Thereby, we dynamically downscale an existing global model simulation to a resolution of 20 km with WRF for the period 1821 CE to 2100 CE.

We find that WRF reproduces the main cyclone hotspots and these results are in line with previous studies (Homar et al., 2007; Raible et al., 2010; Campins et al., 2011). We also find that future cyclone frequency in the Mediterranean is reduced by

https://doi.org/10.5194/egusphere-2025-6315
Preprint. Discussion started: 28 December 2025
© Author(s) 2025. CC BY 4.0 License.

roughly one-third under RCP8.5 conditions. Such a decrease in cyclone frequency in the Mediterranean is also evident in earlier implemented GCMs (Lionello et al., 2002; Bengtsson et al., 2006; Raible et al., 2010; Ulbrich et al., 2013), CMIP5 (Zappa et al., 2014; Hochman et al., 2017), and CMIP6 model simulations (Priestley and Catto, 2022) as well as RCM simulations (Reale et al., 2021). It is thus encouraging that the RCM simulation of this study reproduces this signal. This is, however, to some extent expected as cyclones that form within our domain are still mostly driven by the large-scale weather systems (e.g. pressure systems, jet stream) forced by the global model (Doensen et al., 2025), and hence our RCM likely resembles this.

Besides mean changes, this study focuses on changes in extremes associated with Mediterranean cyclones. Our findings show that cyclones associated with extreme precipitation respond differently in the future in the two subregions, with an increase in extreme precipitation in the WMED and no substantial difference in the EMED. This is remarkable, as CMIP5 simulations project a significant future decrease in mean winter-time precipitation over most of the Mediterranean, except for the northern Mediterranean close to the Alps (Zappa et al., 2015; Reale et al., 2021). Extreme precipitation associated with cyclones show a similar response in CMIP5 simulations (Zappa et al., 2014) and in the RCMs (Reale et al., 2021), although there is quite some spread between the models in the magnitude of the change. Chericoni et al. (2025) showed that RCMs represent wind patterns and air-sea fluxes better, resulting in higher extreme cyclone-related precipitation than in CMIP6 models and thus illustrates the necessity to use high spatial resolution to understand the impact of future climate change on Mediterranean cyclones and the associated extremes as done in this study. Despite no shift in EXC climatology, one difference of the two subregions is that precipitation and compound EXCs in the EMED are shifted southward over the warmer Mediterranean Sea in the future, whereas the average latitude of precipitation EXCs in the WMED remain unchanged in the future. Moreover, the increase in PV for WMED precipitation EXCs during their mature phase is to some extent significant. This increase in PV is partially located around the tropopause in the cold sector indicating a stronger baroclinic cyclone, and within the PV tower in the lower troposphere indicating more diabatic heating. This behaviour is also found for extreme cyclones in idealized simulations (Pfahl et al., 2015; Sinclair et al., 2020). Zhang and Colle (2018) used WRF to study future extratropical cyclones over eastern North America and the western Atlantic at a similar resolution to ours (0.2°). They found that in their initial phase, cyclones are weaker due to climate change, but due to latent heating, they develop rapidly and eventually become stronger than cyclones in the past. This is a similar behavior to the precipitation EXCs in our study, and highlights the impact of latent heating in future warming scenarios.

The assessment of cyclones associated with extreme wind shows that wind EXCs are of similar intensity in the WMED and EMED in our WRF simulation. This finding is in contrast to the driving CESM simulation, where wind EXCs are weaker in the EMED than in the WMED (Doensen et al., 2025). This discrepancy is likely due to rather coarse resolution of $1.9°$ (latitude) $\times$ $2.5°$ (longitude), which is too coarse to reproduce extratropical cyclones in the Mediterranean in an accurate way, as highlighted in Flaounas et al. (2013). Thus, we demonstrate that the dynamical downscaling substantially improves the representation of Mediterranean cyclones.

Concerning climate change, we find a robust increase in wind speed of extreme cyclones in the entire Mediterranean, especially during the mature phase of the EXCs. Compared to the existing literature, the confidence in climate projections related to cyclone-related wind speed is still low (Catto et al., 2019). Moreover, Schemm (2023) demonstrated that the use of kilometer-

https://doi.org/10.5194/egusphere-2025-6315
Preprint. Discussion started: 28 December 2025
© Author(s) 2025. CC BY 4.0 License.

scale climate models may be essential for accurately representing future cyclone tracks, which significantly impact the locations that are impacted most by cyclones. Note also, that most of the existing literature discuss cyclones as a whole, whereas the focus of this study is on extremes. We explain the intensification of wind EXCs in the future projection by changes in the jet stream over the Mediterranean, showing that the wind EXCs are located in the left-exit of an intensified jet streak in the future. In particular, this is found in the mature phase of wind EXCs in the WMED and EMED. Flaounas et al. (2015b) suggested that Mediterranean extreme wind cyclones often co-occur with a strong jet streak south of the cyclone. Moreover, Raveh-Rubin and Wernli (2015) showed that precipitation extremes in the eastern Mediterranean often co-occur with the merging of the midlatitude and subtropical jet in this region, causing cyclogenesis or cyclone intensification. Prezerakos et al. (2005) performed a thorough analysis on the mechanisms behind the cyclone-jet co-occurrence in a case study, showing that an extreme cyclone over the eastern Mediterranean that revived when it was located in the left exit of the subtropical and the right entrance of the midlatitude jet. However, Flaounas et al. (2022) acknowledged that this cyclone-jet co-occurrence has not been studied extensively. Thus, our study contributes to fill this gap by highlighting the importance of the jet position and strength in intensifying extreme cyclones in the Mediterranean.

Furthermore, we investigate the behavior of cyclones associated with compound extreme precipitation and wind. We find that precipitation associated with compound event resemble the climate change signal of precipitation EXCs in both regions of the Mediterranean. However, the wind speed of compound EXCs in the EMED show a strong future reduction. This is in contrast to the intensification of wind speed EXCs in the future.

To conclude, this work offers a comprehensive analysis on the impact of climate change on extreme cyclones and their characteristics in the Mediterranean utilizing a 280 year long dynamically downscaled regional simulation. Our results show evidence that future extreme cyclones will intensify with respect to precipitation and wind speed (most notably in the western Mediterranean) despite a projected reduction in cyclone frequency. Future extreme cyclones tend to be weaker in their initial phase, but intensify more rapidly and remain stronger in their mature phase. Such developments could exacerbate the socioeconomic impacts of cyclones, compounding the effects of climate change in a region projected to be already among the most severely affected worldwide. Still, the number of extreme cyclones examined for each period is relatively small, since our work only consists of a single member simulation. Future work using ensembles from RCMs or km-scale GCMs could further solidify our understanding of future extreme cyclones in the Mediterranean.

Code availability. The cyclone tracking was performed with the detection and tracking scheme of Blender et al. (1997) and is available on request. The other analysis steps were performed with python scripts. As they are standard methods, they are not uploaded to a repository. These scripts are available on request.

Data availability. Post-processed WRF data used for the study are available at https://doi.org/10.5281/zenodo.17965187 Complete WRF data are locally stored and are available upon request

https://doi.org/10.5194/egusphere-2025-6315
Preprint. Discussion started: 28 December 2025
© Author(s) 2025. CC BY 4.0 License.

Author contributions. OD, MM, and CCR contributed to the design of the study. OD carried out the WRF simulations. OD performed the principal analysis and wrote the manuscript under the supervision of CCR. MM, EDT and CCR provided critical feedback on the results and drafted the manuscript together with OD. All authors contributed to the writing and scientific discussion.

Competing interests. The authors declare no conflict of interest.

Acknowledgements. We acknowledge the Swiss National Supercomputing Centre (CSCS) in Lugano, Switzerland, for providing the necessary computational resources and supercomputing architecture to perform the simulations under project IDs 482 and 615. OD and CCR received funding from the Swiss National Science Foundation (grant no. IZCOZ0_205416).

https://doi.org/10.5194/egusphere-2025-6315
Preprint. Discussion started: 28 December 2025
© Author(s) 2025. CC BY 4.0 License.

References

An, K. (1933). Sulla determinazione empirica di una legge didistribuzione. *Giorn Dell'inst Ital Degli Att*, 4:89–91.

Bengtsson, L., Hodges, K. I., and Roeckner, E. (2006). Storm tracks and climate change. *Journal of Climate*, 19(15):3518–3543.

Blender, R., Fraedrich, K., and Lunkeit, F. (1997). Identification of cyclone-track regimes in the north atlantic. *Quarterly Journal of the Royal Meteorological Society*, 123(539):727–741.

Booth, J. F., Naud, C. M., and Jeyaratnam, J. (2018). Extratropical cyclone precipitation life cycles: A satellite-based analysis. *Geophysical Research Letters*, 45(16):8647–8654.

Büeler, D. and Pfahl, S. (2019). Potential vorticity diagnostics to quantify effects of latent heating in extratropical cyclones. part ii: Application to idealized climate change simulations. *Journal of the Atmospheric Sciences*, 76(7):1885–1902.

Campa, J. and Wernli, H. (2012). A pv perspective on the vertical structure of mature midlatitude cyclones in the northern hemisphere. *Journal of the Atmospheric Sciences*, 69(2):725–740.

Campins, J., Genovés, A., Picornell, M., and Jansà, A. (2011). Climatology of mediterranean cyclones using the era-40 dataset. *International Journal of Climatology*, 31(11):1596–1614.

Carniel, C. E., Ricchi, A., Ferretti, R., Curci, G., Miglietta, M. M., Reale, M., Serafini, P., Wellmeyer, E. D., Davolio, S., Zardi, D., and Kantha, L. (2024). A high-resolution climatological study of explosive cyclones in the mediterranean region: Frequency, intensity and synoptic drivers. *Quarterly Journal of the Royal Meteorological Society*, 150(765):5561–5582.

Catto, J. L., Ackerley, D., Booth, J. F., Champion, A. J., Colle, B. A., Pfahl, S., Pinto, J. G., Quinting, J. F., and Seiler, C. (2019). The future of midlatitude cyclones. *Current Climate Change Reports*, 5:407–420.

Chericoni, M., Fosser, G., Flaounas, E., Gaetani, M., and Anav, A. (2025). Unravelling drivers of the future mediterranean precipitation paradox during cyclones. *npj Climate and Atmospheric Science*, 8(1).

Danielson, J. J. and Gesch, D. B. (2011). *Global multi-resolution terrain elevation data 2010 (GMTED2010)*.

Davis, C. A. and Emanuel, K. A. (1991). Potential vorticity diagnostics of cyclogenesis. *Monthly Weather Review*, 119(8):1929–1953.

Doensen, O., Messmer, M., Kim, W. M., and Raible, C. C. (2025). Characterization of the mean and extreme mediterranean cyclones and their variability during the period 1500 bce to 1850 ce. *Climate of the Past*, 21(7):1305–1322.

Dolores-Tesillos, E., Teubler, F., and Pfahl, S. (2022). Future changes in north atlantic winter cyclones in cesm-le – part 1: Cyclone intensity, potential vorticity anomalies, and horizontal wind speed. *Weather and Climate Dynamics*, 3(2):429–448.

Dudhia, J. (1989). Numerical study of convection observed during the winter monsoon experiment using a mesoscale two-dimensional model. *Journal of the Atmospheric Sciences*, 46(20):3077–3107.

Ferrarin, C., Bajo, M., Benetazzo, A., Cavaleri, L., Chiggiato, J., Davison, S., Davolio, S., Lionello, P., Orlić, M., and Umgiesser, G. (2021). Local and large-scale controls of the exceptional venice floods of november 2019. *Progress in Oceanography*, 197:102628.

Fita, L., Romero, R., and Ramis, C. (2006). Intercomparison of intense cyclogenesis events over the mediterranean basin based on baroclinic and diabatic influences. *Advances in Geosciences*, 7:333–342.

Flaounas, E., Davolio, S., Raveh-Rubin, S., Pantillon, F., Miglietta, M. M., Gaertner, M. A., Hatzaki, M., Homar, V., Khodayar, S., Korres, G., et al. (2022). Mediterranean cyclones: Current knowledge and open questions on dynamics, prediction, climatology and impacts. *Weather and Climate Dynamics*, 3(1):173–208.

Flaounas, E., Drobinski, P., and Bastin, S. (2013). Dynamical downscaling of ipsl-cm5 cmip5 historical simulations over the mediterranean: benefits on the representation of regional surface winds and cyclogenesis. *Climate dynamics*, 40:2497–2513.

https://doi.org/10.5194/egusphere-2025-6315
Preprint. Discussion started: 28 December 2025
© Author(s) 2025. CC BY 4.0 License.

Flaounas, E., Kotroni, V., Lagouvardos, K., and Flaounas, I. (2014). Cyclotrack (v1. 0)–tracking winter extratropical cyclones based on relative vorticity: sensitivity to data filtering and other relevant parameters. *Geoscientific Model Development*, 7(4):1841–1853.

Flaounas, E., Lagouvardos, K., Kotroni, V., Claud, C., Delanoë, J., Flamant, C., Madonna, E., and Wernli, H. (2015a). Processes leading to heavy precipitation associated with two mediterranean cyclones observed during the hymex sop1. *Quarterly Journal of the Royal Meteorological Society*, 142(S1):275–286.

Flaounas, E., Raveh-Rubin, S., Wernli, H., Drobinski, P., and Bastin, S. (2015b). The dynamical structure of intense mediterranean cyclones. *Climate Dynamics*, 44:2411–2427.

Givon, Y., Hess, O., Flaounas, E., Catto, J. L., Sprenger, M., and Raveh-Rubin, S. (2024). Process-based classification of mediterranean cyclones using potential vorticity. *Weather and Climate Dynamics*, 5(1):133–162.

Hochman, A., Alpert, P., Kunin, P., Rostkier-Edelstein, D., Harpaz, T., Saaroni, H., and Messori, G. (2020). The dynamics of cyclones in the twentyfirst century: the eastern mediterranean as an example. *Climate Dynamics*, 54:561–574.

Hochman, A., Harpaz, T., Saaroni, H., and Alpert, P. (2017). Synoptic classification in 21st century cmip5 predictions over the eastern mediterranean with focus on cyclones. *International Journal of Climatology*, 38(3):1476–1483.

Homar, V., Jansà, A., Campins, J., Genovés, A., and Ramis, C. (2007). Towards a systematic climatology of sensitivities of mediterranean high impact weather: a contribution based on intense cyclones. *Natural Hazards and Earth System Sciences*, 7(4):445–454.

Homar, V., Ramis, C., and Alonso, S. (2002). A deep cyclone of african origin over the western mediterranean: diagnosis and numerical simulation. *Annales Geophysicae*, 20(1):93–106.

Hong, S.-Y., Noh, Y., and Dudhia, J. (2006). A new vertical diffusion package with an explicit treatment of entrainment processes. *Monthly Weather Review*, 134(9):2318–2341.

Hurrell, J. W., Holland, M. M., Gent, P. R., Ghan, S., Kay, J. E., Kushner, P. J., Lamarque, J.-F., Large, W. G., Lawrence, D., Lindsay, K., et al. (2013). The community earth system model: a framework for collaborative research. *Bulletin of the American Meteorological Society*, 94(9):1339–1360.

IPCC (2021). *Climate Change 2021: The Physical Science Basis. Contribution of Working Group I to the Sixth Assessment Report of the Intergovernmental Panel on Climate Change*. Cambridge University Press, Cambridge, UK and New York, NY, USA.

Jerez, S., López-Romero, J. M., Turco, M., Lorente-Plazas, R., Gómez-Navarro, J. J., Jiménez-Guerrero, P., and Montávez, J. P. (2020). On the spin-up period in wrf simulations over europe: Trade-offs between length and seasonality. *Journal of Advances in Modeling Earth Systems*, 12(4).

Jiménez, P. A., Dudhia, J., González-Rouco, J. F., Navarro, J., Montávez, J. P., and García-Bustamante, E. (2012). A revised scheme for the wrf surface layer formulation. *Monthly Weather Review*, 140(3):898–918.

Kain, J. S. (2004). The kain–fritsch convective parameterization: An update. *Journal of Applied Meteorology*, 43(1):170–181.

Kim, W. M., Blender, R., Sigl, M., Messmer, M., and Raible, C. C. (2021). Statistical characteristics of extreme daily precipitation during 1501 bce–1849 ce in the community earth system model. *Climate of the Past*, 17(5):2031–2053.

Lionello, P., Conte, D., and Reale, M. (2019). The effect of cyclones crossing the mediterranean region on sea level anomalies on the mediterranean sea coast. *Natural Hazards and Earth System Sciences*, 19(7):1541–1564.

Lionello, P., Dalan, F., and Elvini, E. (2002). Cyclones in the mediterranean region: the present and the doubled co2 climate scenarios. *Climate Research*, 22:147–159.

Martius, O., Pfahl, S., and Chevalier, C. (2016). A global quantification of compound precipitation and wind extremes. *Geophysical Research Letters*, 43(14):7709–7717.

https://doi.org/10.5194/egusphere-2025-6315
Preprint. Discussion started: 28 December 2025
© Author(s) 2025. CC BY 4.0 License.

Messmer, M. and Simmonds, I. (2021). Global analysis of cyclone-induced compound precipitation and wind extreme events. *Weather and Climate Extremes*, 32:100324.

Mlawer, E. J., Taubman, S. J., Brown, P. D., Iacono, M. J., and Clough, S. A. (1997). Radiative transfer for inhomogeneous atmospheres: Rrtm, a validated correlated-k model for the longwave. *Journal of Geophysical Research: Atmospheres*, 102(D14):16663–16682.

Neu, U., Akperov, M. G., Bellenbaum, N., Benestad, R., Blender, R., Caballero, R., Cocozza, A., Dacre, H. F., Feng, Y., Fraedrich, K., Grieger, J., Gulev, S., Hanley, J., Hewson, T., Inatsu, M., Keay, K., Kew, S. F., Kindem, I., Leckebusch, G. C., Liberato, M. L. R., Lionello, P., Mokhov, I. I., Pinto, J. G., Raible, C. C., Reale, M., Rudeva, I., Schuster, M., Simmonds, I., Sinclair, M., Sprenger, M., Tilinina, N. D., Trigo, I. F., Ulbrich, S., Ulbrich, U., Wang, X. L., and Wernli, H. (2013). Imilast: A community effort to intercompare extratropical cyclone detection and tracking algorithms. *Bulletin of the American Meteorological Society*, 94(4):529–547.

Nissen, K., Leckebusch, G., Pinto, J. G., Renggli, D., Ulbrich, S., and Ulbrich, U. (2010). Cyclones causing wind storms in the mediterranean: characteristics, trends and links to large-scale patterns. *Natural Hazards and Earth System Sciences*, 10(7):1379–1391.

Nissen, K. M., Leckebusch, G. C., Pinto, J. G., and Ulbrich, U. (2014). Mediterranean cyclones and windstorms in a changing climate. *Regional environmental change*, 14:1873–1890.

Niu, G.-Y., Yang, Z.-L., Mitchell, K. E., Chen, F., Ek, M. B., Barlage, M., Kumar, A., Manning, K., Niyogi, D., Rosero, E., Tewari, M., and Xia, Y. (2011). The community noah land surface model with multiparameterization options (noah-mp): 1. model description and evaluation with local-scale measurements. *Journal of Geophysical Research*, 116(D12).

Pettersen, S. (1956). *Weather Analysis and Forecasting: Volume I: Motion and Motion Systems*. McGraw-Hill, New York, USA.

Pfahl, S., O'Gorman, P. A., and Singh, M. S. (2015). Extratropical cyclones in idealized simulations of changed climates. *Journal of Climate*, 28(23):9373–9392.

Pfahl, S. and Sprenger, M. (2016). On the relationship between extratropical cyclone precipitation and intensity. *Geophysical Research Letters*, 43(4):1752–1758.

Pfahl, S. and Wernli, H. (2012). Quantifying the relevance of cyclones for precipitation extremes. *Journal of Climate*, 25(19):6770–6780.

Portal, A., Raveh-Rubin, S., Catto, J. L., Givon, Y., and Martius, O. (2024). Linking compound weather extremes to mediterranean cyclones, fronts and air-streams. *EGUsphere*, 2024:1–24.

Prezerakos, N. G., Flocas, H. A., and Brikas, D. (2005). The role of the interaction between polar and subtropical jet in a case of depression rejuvenation over the eastern mediterranean. *Meteorology and Atmospheric Physics*, 92(1–2):139–151.

Priestley, M. D. K. and Catto, J. L. (2022). Future changes in the extratropical storm tracks and cyclone intensity, wind speed, and structure. *Weather and Climate Dynamics*, 3(1):337–360.

Raible, C., Yoshimori, M., Stocker, T., and Casty, C. (2007). Extreme midlatitude cyclones and their implications for precipitation and wind speed extremes in simulations of the maunder minimum versus present day conditions. *Climate Dynamics*, 28:409–423.

Raible, C. C., Della-Marta, P. M., Schwierz, C., Wernli, H., and Blender, R. (2008). Northern hemisphere extratropical cyclones: A comparison of detection and tracking methods and different reanalyses. *Monthly Weather Review*, 136(3):880–897.

Raible, C. C., Messmer, M., Lehner, F., Stocker, T. F., and Blender, R. (2018). Extratropical cyclone statistics during the last millennium and the 21st century. *Climate of the Past*, 14(10):1499–1514.

Raible, C. C., Ziv, B., Saaroni, H., and Wild, M. (2010). Winter synoptic-scale variability over the mediterranean basin under future climate conditions as simulated by the echam5. *Climate Dynamics*, 35:473–488.

Raveh-Rubin, S. and Flaounas, E. (2017). A dynamical link between deep atlantic extratropical cyclones and intense mediterranean cyclones. *Atmospheric Science Letters*, 18(5):215–221.

https://doi.org/10.5194/egusphere-2025-6315
Preprint. Discussion started: 28 December 2025
© Author(s) 2025. CC BY 4.0 License.

Raveh-Rubin, S. and Wernli, H. (2015). Large-scale wind and precipitation extremes in the mediterranean: a climatological analysis for 1979–2012. *Quarterly Journal of the Royal Meteorological Society*, 141(691):2404–2417.

Reale, M., Cabos Narvaez, W. D., Cavicchia, L., Conte, D., Coppola, E., Flaounas, E., Giorgi, F., Gualdi, S., Hochman, A., Li, L., Lionello, P., Podrascanin, Z., Salon, S., Sanchez-Gomez, E., Scoccimarro, E., Sein, D. V., and Somot, S. (2021). Future projections of mediterranean cyclone characteristics using the med-cordex ensemble of coupled regional climate system models. *Climate Dynamics*, 58(9–10):2501–2524.

Schemm, S. (2023). Toward eliminating the decades-old "too zonal and too equatorward" storm-track bias in climate models. *Journal of Advances in Modeling Earth Systems*, 15(2).

Scherrmann, A., Wernli, H., and Flaounas, E. (2023). Origin of low-tropospheric potential vorticity in mediterranean cyclones. *Weather and Climate Dynamics*, 4(1):157–173.

Scherrmann, A., Wernli, H., and Flaounas, E. (2024). The upstream–downstream connection of north atlantic and mediterranean cyclones in semi-idealized simulations. *Weather and Climate Dynamics*, 5(1):419–438.

Schneidereit, A., Blender, R., and Fraedrich, K. (2010). A radius–depth model for midlatitude cyclones in reanalysis data and simulations. *Quarterly Journal of the Royal Meteorological Society*, 136(646):50–60.

Sinclair, V. A., Rantanen, M., Haapanala, P., Räisänen, J., and Järvinen, H. (2020). The characteristics and structure of extra-tropical cyclones in a warmer climate. *Weather and Climate Dynamics*, 1(1):1–25.

Skamarock, C., Klemp, B., Dudhia, J., Gill, O., Liu, Z., Berner, J., Wang, W., Powers, G., Duda, G., Barker, D., and Huang, X.-y. (2021). A Description of the Advanced Research WRF Model Version 4.3.

Thompson, G., Field, P. R., Rasmussen, R. M., and Hall, W. D. (2008). Explicit forecasts of winter precipitation using an improved bulk microphysics scheme. part ii: Implementation of a new snow parameterization. *Monthly Weather Review*, 136(12):5095–5115.

Trigo, I. F. (2006). Climatology and interannual variability of storm-tracks in the euro-atlantic sector: a comparison between era-40 and ncep/ncar reanalyses. *Climate Dynamics*, 26(2-3):127–143.

Trigo, I. F., Davies, T. D., and Bigg, G. R. (1999). Objective climatology of cyclones in the mediterranean region. *Journal of Climate*, 12(6):1685–1696.

Trigo, I. F., Davies, T. D., and Bigg, G. R. (2000). Decline in mediterranean rainfall caused by weakening of mediterranean cyclones. *Geophysical Research Letters*, 27(18):2913–2916.

Ulbrich, U., Leckebusch, G. C., Grieger, J., Schuster, M., Akperov, M., Bardin, M. Y., Feng, Y., Gulev, S., Inatsu, M., Keay, K., Kew, S. F., Liberato, M. L., Lionello, P., Mokhov, I. I., Neu, U., Pinto, J. G., Raible, C. C., Reale, M., Rudeva, I., Simmonds, I., Tilinina, N. D., Trigo, I. F., Ulbrich, S., and Wang (2013). Are greenhouse gas signals of northern hemisphere winter extra-tropical cyclone activity dependent on the identification and tracking algorithm? *Meteorologische Zeitschrift*, 22(1):61–68.

Vakrat, E. and Hochman, A. (2023). Dynamical systems insights on cyclonic compound "wet" and "windy" extremes in the eastern mediterranean. *Quarterly Journal of the Royal Meteorological Society*, 149(757):3593–3606.

Welch, B. L. (1947). The generalization of 'student's'problem when several different population varlances are involved. *Biometrika*, 34(1-2):28–35.

Willison, J., Robinson, W. A., and Lackmann, G. M. (2013). The importance of resolving mesoscale latent heating in the north atlantic storm track. *Journal of the Atmospheric Sciences*, 70(7):2234–2250.

Zappa, G., Hawcroft, M. K., Shaffrey, L., Black, E., and Brayshaw, D. J. (2014). Extratropical cyclones and the projected decline of winter mediterranean precipitation in the cmip5 models. *Climate Dynamics*, 45(7–8):1727–1738.

https://doi.org/10.5194/egusphere-2025-6315
Preprint. Discussion started: 28 December 2025
© Author(s) 2025. CC BY 4.0 License.

Zappa, G., Hoskins, B. J., and Shepherd, T. G. (2015). The dependence of wintertime mediterranean precipitation on the atmospheric circulation response to climate change. *Environmental Research Letters*, 10(10):104012.

Zappa, G., Shaffrey, L. C., Hodges, K. I., Sansom, P. G., and Stephenson, D. B. (2013). A multimodel assessment of future projections of
595 north atlantic and european extratropical cyclones in the cmip5 climate models*. *Journal of Climate*, 26(16):5846–5862.

Zhang, Z. and Colle, B. A. (2018). Impact of dynamically downscaling two cmip5 models on the historical and future changes in winter extratropical cyclones along the east coast of north america. *Journal of Climate*, 31(20):8499–8525.

Zscheischler, J., Westra, S., Van Den Hurk, B. J., Seneviratne, S. I., Ward, P. J., Pitman, A., AghaKouchak, A., Bresch, D. N., Leonard, M., Wahl, T., et al. (2018). Future climate risk from compound events. *Nature climate change*, 8(6):469–477.